Polyamorphic transition in a transition metal based metallic glass under high pressure

Qing Du, Xiong-Jun Liu, Qiaoshi Zeng, Huiyang Fan, Hui Wang, Yuan Wu, Shi-Wei Chen, and Zhao-Ping Lu

Phys. Rev. B **99**, 014208 — Published 24 January 2019

DOI: 10.1103/PhysRevB.99.014208

Polyamorphic transition in a transition metal-based metallic glass under high pressure

Qing Du,[1,] Xiong-Jun Liu,[1, *] Qiaoshi Zeng,[2,3] Huiyang Fan,[1] Hui Wang,[1] Yuan Wu,[1] Shi-Wei Chen,[4] Zhao-Ping Lu,[1,*]

[1]State Key Laboratory for Advanced Metals and Materials, University of Science and Technology Beijing, Beijing 100083, China.
[2]Center for High Pressure Science and Technology Advanced Research, Pudong, Shanghai 201203, China.
[3] Jiangsu Key Laboratory of Advanced Metallic Materials, School of Materials Science and Engineering, Southeast University, Nanjing 211189, China.
[4]National Synchrotron Radiation Research Center (NSRRC), Hsinchu 30076, Taiwan, China

Abstract

Pressure-induced glass-glass transition (GGT) has been reported in a few rare-earth based and main-group metallic glasses (MGs), and during which, the compressibility decreases with the transformation from a low-density to a high-density amorphous state. Herein, we report an unexpected GGT behavior in Pd-based MGs under pressure, which is characterized by an anomalous increase in the compressibility with the pressure. State-of-the-art high-energy synchrotron technique, coupled with theoretical simulations, reveals that this unique GGT behavior is primarily caused by the change in bonding characteristics, i.e., some covalent-like atomic bonds in the as-prepared state change to metallic ones under high pressure, which also leads to the increase in the compressibility. Our current findings shed new light on understanding the nature of polyamorphic transitions in MGs.

*To whom correspondence should be addressed. E-mail: xjliu@ustb.edu.cn (X.J. Liu) or luzp@ustb.edu.cn (Z.P. Lu); Tel: +86-10-8237 5387

I. INTRODUCTION

Pressure, one of the basic thermodynamic parameters, has been demonstrated as an important means to modulate atomic structure and properties of materials [1-4]. Pressure-induced polyamorphism transitions (PTs) have been reported in various amorphous matters, especially in those glasses with directional bonds and open structures. Similar to the transformation from the low-density to the high-density amorphous ice in glassy water, a series of oxide and chalcogenide glasses was found to undergo a densification process under high pressure. For example, the density of $GeSe_4$ glass increased significantly when it was subjected to a hydro-pressure of 3 GPa [5]. The densification process in these network-forming glasses is associated with the fact that the open atomic structure collapses into more densely packed structures under high pressure.

District from traditional oxide and chalcogenide glasses, metallic glasses (MGs) possess dense atomic packing with non-directional metallic bonds, which are unfavorable for the pressure-induced PT. However, pressure-induced GGTs have still been reported in few special MGs due to the delocalization of *f*-electrons or the enhancement of covalent interactions [6-18], which are characterized by discontinuous changes in physical properties with pressure, such as compressibility, density, electrical resistivity and modulus. Typically, the bulk modulus increases along with the volume shrinkage under pressure while the compressibility (i.e., the slope of the volume-pressure curve) suddenly decreases right after the occurrence of GGT at a certain pressure. It can be rationalized that the high-density glass state becomes more difficult to shrink in terms of the stronger atomic interactions. As a matter of fact, all reported pressure-induced GGTs were accompanied with the decreased compressibility, although elastic anomalies with the increase of pressure were reported in a rare-earth based MG [19].

In this *letter*, we report an unprecedented GGT behavior in Pd-Ni-P MGs with an unusual increase in compressibility as the applied pressure increases. State-of-the-art high-energy synchrotron radiation x-ray technique combined with diamond anvil cell (DAC) apparatus and first-principles calculations reveal that such unique GGT is primarily originated from the change of bonding characteristics from covalent-like to metallic bonds under high pressure. The current findings have important implications for understanding the polyamorphic transitions of amorphous matters in general.

II. EXPERIMENTAL AND COMPUTATIONAL DETAILS

Master ingots were prepared by arc-melting a mixture of pure Pd and the Ni-P pre-alloy in an argon atmosphere. Alloy ingots were fluxed with B_2O_3 at 1273 K for 4 h. $Pd_{41.5}Ni_{41.5}P_{17}$ glassy ribbons with a cross-section of 0.05×8 mm^2 were produced via a single copper roller melt-spinning under argon atmosphere. The samples were cut into about $50 \times 50 \times 12$ μm^3 chips, and then were loaded into a symmetrical DAC along with tiny ruby balls ruby around the sample as a pressure calibrant [20]. The 4:1 methanol-ethanol mixture (volume ratio) or helium were used as the pressure medium to ensure hydrostatic pressure condition. The pressure of the methanol-ethanol mixture was used below 10 GPa to avoid the influence of non-hydrostaticity [21]. In situ high-pressure angle-dispersive x-ray diffraction (XRD) experiments with a focused x-ray beam of ~15 × ~15 μm^2 were performed at the beamline 16-ID-B and 16-BM-D of the High-Pressure Collaborative Access Team (HPCAT), Advanced Photon Source (APS), Argonne National Laboratory (ANL), and also at the beamline

12.2.2, Advanced light source (ALS), Lawrence Berkeley National Laboratory (LBNL). Pair distribution function (PDF) at ambient pressure was measured at beamline 11-ID-C, APS, ANL. The extended X-ray absorption fine structure (EXAFS) spectroscopy of Pd, Ni and P K-edge were recorded at beamline BL01C2, in NSRRC, Taiwan, and also at beamline 20-BMB, APS, ANL. Experimental data were analyzed by using Athena and Artemis software package [22].

The *ab initial* molecular dynamics (AIMD) simulations with a canonical NPT were conducted by the density functional theory (DFT)-based Vienna ab-initio simulation package (VASP) [23] using projector augmented waves (PAW) [24] to obtain the atomic structure of the $Pd_{41.5}Ni_{41.5}P_{17}$ glass. The generalized gradient approximation of Perdew-Burke-Ernzerh of (GGA-PBE) was adopted for the exchange correlation functional [25]. The cooling process was performed on the Gamma point only, and the electronic properties were calculated with a 5 × 5 × 5 k-point mesh. A cubic supercell containing 200 atoms was initially constructed with a periodic boundary condition. The system was firstly melted and equilibrated at 2000 K for 4000 steps with a time step of 5 fs, and then quenched down to 300 K with a cooling rate of $\sim 10^{13}$ K/s. Finally, the glass state was relaxed for 50 ps under zero external pressure at 300 K to get a fully relaxed $Pd_{41.5}Ni_{41.5}P_{17}$ glass. The simulation density of the supercell at 300 K is in good agreement with the experimental data (0.0778 $Å^{-3}$). The reliability of the AIMD-atomic structure was also verified by the XRD and EXAFS spectra. The hydrostatic pressures were imposed on the configuration by reducing the cell size gradually to explore the pressure effect. At each pressure, 2000 configurations were collected to calculate pair distribution functions (PDFs) and partial PDFs. The visualization of atomic and electronic structures was performed by VESTA. [26]

III. RESULTS AND DISCUSSION

A. *In-situ* high-pressure X-ray diffraction data

Fig. 1a shows in-situ high pressure X-ray diffraction patterns during pressurization for the as-cast $Pd_{41.5}Ni_{41.5}P_{17}$ MG, where XRD patterns were collected up to 10.5(1) GPa in methanol-ethanol mixture and 22.6(1) GPa in helium. Only diffuse halos with no sharp Bragg peaks were observed, indicating that the sample remains a fully amorphous state under the applied pressures. The arrows in **Fig. 1a** show that the first sharp diffraction peak (FSDP) shifts towards the high q side with increasing pressure, which reflects the densification effect of pressure according to the power law relationship between the FSDP position $2\pi/q_1$ and atomic volume [27, 28]. This result is consistent with all previous reports.

Figure 1b shows the evolution of relative volume V_{Pr}/V_0 with pressure, where V_{Pr} and V_0 are the volume under a certain applied pressure of P_{r} and ambient pressure, respectively. As can be seen, the volume decreases as the applied pressure increases, demonstrating a normal pressure-induced densification process, as reported in previous studies [6-19]. A total shrinkage in volume is estimated to be about 9% when the pressure is increased to 22.6(1) GPa. By carefully analyzing the data, we found that the data points could not be fitted by a single linear function (cf. **Fig. 1b**). Instead, the evolution of relative volume V_{Pr}/V_0 with pressure obeys with two different equation of states (EOSs) [29], as indicated respectively by the black and red dashed lines in **Fig. 1b**. The two EOSs were analyzed using a third-order Birch-Murnaghan relation:

$$\mathrm{p} = \frac{3}{2} B_0 \left[\left(\frac{V_{Pr}}{V_0} \right)^{-\frac{7}{3}} - \left(\frac{V_{Pr}}{V_0} \right)^{-\frac{5}{3}} \right] \left\{ 1 - \frac{3}{4} \left(4 - B_0^{'} \right) \left[\left(\frac{V_{Pr}}{V_0} \right)^{-\frac{2}{3}} - 1 \right] \right\}. \tag{1}$$

Where B_0 and B_0' are the bulk modulus and its pressure derivative at zero pressure, respectively. The B_0' is fixed at 4, which is often adopted for glassy solids [30]. As shown in Table I, the resultant B_0 below 6 GPa is 37.1% larger than that above 6 GPa, identifying the increased compressibility with pressure. Both the reduced chi-square and R-square values indicate that the fitting is reasonable. This result clearly reveals the existence of pressure-induced GGT in the $Pd_{41.5}Ni_{41.5}P_{17}$ MG. The transition pressure was determined to be ~6 GPa by the intersection of the two EOSs as shown in **Fig. 1b**. More interestingly, we found that the slope of volume-pressure curve for the pressure regime above 6 GPa is larger than that for the pressure regime below 6 GPa. Meanwhile, the bulk modulus B_0 above 6 GPa is smaller than that below 6 GPa, implying that the compressibility is enhanced as the density increases accompanying with the GGT. This phenomenon is totally different from all previous GGTs reported in MGs, where the compressibility is commonly decreased with increasing pressure/density.

B. Total density of states (DOS) and the projected DOS

To understand the underlying mechanism responsible for the above abnormal behavior, we conducted density-function-theory (DFT) based molecular dynamics simulations and electronic structure calculations. **Figure 2** shows the simulated atomic structures of the $Pd_{41.5}Ni_{41.5}P_{17}$ glass at 300 K under zero pressure, which is verified by the experimental structure determined by high-energy synchrotron XRD and EXAFS measurements. As shown in **Figs. 2b-d**, the pair distribution function (PDF) and EXAFS spectra of the simulated atomic configuration at 300 K agree well with our experimental data at the ambient environment, confirming that the simulated atomic structure is reliable. The hydrostatic pressures were imposed on the configuration by reducing the cell size gradually to explore the pressure effect on electronic structures.

With these configurations, we calculated the electronic structures of total density of states (DOS) and the projected DOS (PDOS) of the $Pd_{41.5}Ni_{41.5}P_{17}$ MG under ambient and high pressures. In order to clearly distinguish the difference in electronic structures between the initial state and the compressed one, we extended the high pressure to 78 GPa, considering the fact that the simulated pressure is often exploited to be much larger than the experimental ones in previous studies [31, 32]. As shown in **Fig. 3a** (the black line), the resultant DOS at ambient pressure, which is consistent with previous studies [33, 34], can be divided into four kinds of bands in terms of its profile: the band I at -15 eV $< E-E_F <$ -10 eV (E_F is the Fermi energy), band II at -10 eV $< E-E_F <$ -5 eV, band III at -5 eV $< E-E_F <$ 0 eV, and IV at $E-E_F >0$ eV. By carefully analyzing the PDOS curves of Pd, Ni and P components (**Figs. 3b-d**), it is clear that the band I results mainly from the 3s electrons of P atoms and their hybridization with the s electrons of Ni and Pd atoms. The band II is attributed to the hybridization between the p electron of P atoms and the s and d electrons of Ni and Pd atoms. Note that the bandwidth of band I and II is significantly narrower than those in pure metals [33], implying the localization of electrons lies in-between P and Pd/Ni nuclei. The band III is mainly consisted of s and d electrons of Ni and Pd as well as a small amount of the P component. Obviously, there is a “pseudogap” at about -5 eV between the band II and III in the total DOS curve and a visible gap in the s and d electrons of Ni and Pd atoms in the PDOS, indicating again that partial s and d electrons of Ni and Pd atoms become localized due to the orbital hybridization. The band IV is constructed by the anti-bonding states of s- and d-orbitals of Ni and Pd atoms, corresponding to the bonding states in band II and III. The presence of bonding and antibonding as well as the "pseudogap" indicate the covalent-dominant bonding of P with Pd/Ni [34] do exist in the as-cast $Pd_{41.5}Ni_{41.5}P_{17}$ glass, which is consistent with the previous claim about the coexistence of covalent-like and metallic bonds in the Pd-Ni-P MGs [33-35].

Based on the above results, it seems that the pressure effect on the current GGT is closely related to the electronic structures in the MG. As shown in **Fig. 3a**, the DOS profile varies significantly when the configuration was imposed with a high pressure of 78 GPa. In particular, the band III is broadened with the lower bound shifting from -5 to -7.5 eV. More importantly, the "pseudogap" between the band II and III tends to disappear and the profile of band II and III becomes similar with that of typical metals [33] as the pressure increases. These results suggest that the localization of s- and d-electrons of Pd and Ni is reduced whilst the development of metallic bonding is enhanced in the high-pressured $Pd_{41.5}Ni_{41.5}P_{17}$ MG. Moreover, the high pressure makes the s- and p-orbitals of P shift to the lower energy band (**Fig. 3c**). Meanwhile, the intensity of these orbitals dropped by more than 25% compared to that under ambient pressure, indicating the weakening of the covalent bonds bearing s- and p-electrons of P. On the other hand, the pressure-induced widening of the energy band of s- and d-orbitals for the Ni and Pd appears, suggesting that some localized s- and d-electrons of Ni and Pd which participate in covalent bonds turns to delocalize to form metallic bonds.

C. Different charge density distribution and electron localization function

The covalent-like bonding between P and Pd/Ni and the pressure-induced bonding-type transformation behavior can further be revealed by different charge density distribution and electron localization function (ELF) [36], as shown in **Fig. 4 and 5**. From **Fig. 4a**, distinct sharing electrons in-between P and Pd/Ni are seen, which is typical for covalent bonding. In addition, the ELF iso-surface with a value larger than 0.5 is mainly distributed around P atoms (see **Fig. 5a**), which also verifies the covalence-dominated bonding behavior of P associated bonds. As the pressure increases from 0 to 41 GPa (**Figs. 4a-c**), the electronic density shared by P and Ni/Pd decreases slightly. However, a significant reduction of the shared electronic density appears when the pressure reaches 78 GPa **(Fig. 4d**). Accordingly, the corresponding ELF value is reduced significantly in the high-pressure configuration with respect to the as-quenched counterpart (**Fig. 5**). These results unambiguously uncover that there exists a change from covalent-dominant to metallic-dominant bonding behavior in the $Pd_{41.5}Ni_{41.5}P_{17}$ glass under pressure. It is well known that covalent bonds are rigid due to the characteristics of saturation and directionality, whilst metallic bonds are flexible due to the itinerant feature of valence electrons. As a result, the covalent bond is always much stiffer and more difficult to deform than metallic bonds with the same constituents. Therefore, it can be rationalized that the pressure-induced change from covalent-dominant to metallic-dominant bonds is responsible for the unusual increase of compressibility with pressure.

D. Pair distribution functions under different pressures

Based on the computation results, the evolution of the total and partial PDFs with pressure is shown in **Fig. 6**. A shoulder at about 2.27 Å appears (indicated by the yellow arrow in **Fig. 6a**) while the first peak is located at about 2.67 Å in the PDF under 0 GPa, which is consistent with previous reports [34]. The partial PDFs of P-(Pd, Ni), Ni-(Pd, Ni) and Pd-(Pd, Ni) correlations in the $Pd_{41.5}Ni_{41.5}P_{17}$ glass are illustrated in **Figs. 6b-d**. The first peak in the partial PDF of P-(Pd, Ni) under 0 GPa is centered at about 2.26 Å, which is in good agreement with the shoulder position in the total PDF, manifesting that the shoulder in the total PDF is originated from the bonding between P and Ni/Pd atoms (marked as P-M in **Fig. 5a**). The position of the first peaks in the partial PDFs of Ni-(Pd, Ni) and Pd-(Pd, Ni) correlations under 0 GPa is at 2.61 Å and 2.72 Å, respectively, which is close to that of the first peak in the total PDF, implying that the main peak in the total PDF is consisted of the (Pd, Ni)-(Ni, Pd) bonding (marked as M-M in **Fig. 5a**).

The position of the first peak of the total PDF shifts to a lower *r* value with the increase of pressure, as indicated by the arrow in the inset of **Fig. 6a**. The peak position decreases from 2.67 Å under 0 GPa to 2.43 Å under 78 GPa, verifying the densification process. More importantly, the shoulder becomes weak with the increase of pressure. As illustrated above, the shoulder results from the formation of the Ni-P and Pd-P bonding. From **Fig. 6b**, one can see that the intensity of the first peak of the P-(Ni, Pd) PDF decreases with the increase of pressure, indicating the reduction of P-(Ni, Pd) pairs, which is consistent with the weakening of shoulder in the total PDF. By contrast, M-M atomic pairs increase along with the increase of pressure, as evidenced by the enhanced peak intensity of the M-M PDFs under high pressure (**Figs. 6c and 6d**). As demonstrated by electronic structure analysis (**Figs. 3-5**), covalent bonding exists in the atomic pairs between P and Pd/Ni in the $Pd_{41.5}Ni_{41.5}P_{17}$ MG. In this regard, the decrease in the intensity of the P-M pairs evidently manifests the pressure-induced weakening of covalent bonding, whereas the enhancement in the intensity of M-M pairs certifies the strengthening of metallic bonding. Therefore, the evolution of the total and partial

PDFs with pressure also demonstrates the change of bonding characteristics from covalent-like to metallic bonds under high pressure.

E. Comparison with previous GGTs induced by *f*-electron delocalization

GGTs have been reported in a few rare-earth-based MGs, where apparent bond shortening and volume collapses were observed due to the *f*-electron delocalization induced by pressure. The bond shortening and volume collapse lead to the stronger bonds and the smaller compressibility of the high-pressured state. Although the anomalous softening of bulk modulus with pressure was also observed at the initial stage during pressurization in few Ce-based MGs [37], the GGT was usually accompanied by the increase of compressibility, as expected by the common notion. In contrast, there is no apparent bond shortening and volume collapse in our case due to the absence of *f* electrons (shown in **Fig. 1b**). More interestingly, the unique polyamorphic transition is accompanied with an increased compressibility under high pressure, which sidesteps the paradigm of decreasing compressibility with pressure. The compelling evidences from our comprehensive electronic structural analyses (**Figs. 3-5**) demonstrate that this unprecedented phenomenon originates from the change from covalent-dominant to metallic-dominant bonding behavior under pressure. Similar with previous pressure-induced GGTs, the current one observed in the $Pd_{41.5}Ni_{41.5}P_{17}$ MG is also reversible as the pressure released, as evidenced by the fact that the first sharp diffraction peak position of the sample after pressure release from 10.5(1) GPa is almost identical with that before pressurization (**Fig. 7**).

V. SUMMARY

To sum up, by employing the *in-situ* high pressure X-ray diffraction under hydrostatic pressure conditions, we discovered an anomalous polyamorphic transition in the $Pd_{41.5}Ni_{41.5}P_{17}$ MG at around 6 GPa, which is characterized by the increase in the compressibility under high pressure. The electronic structure analysis indicates that there exists the covalent bonding between P and Pd/Ni atoms in the as-cast $Pd_{41.5}Ni_{41.5}P_{17}$ glass. Under high pressure, the covalent-dominant bonds change to metallic-dominant ones, which leads to the unusual increase in the compressibility with pressure. The observed GGT behavior and the related mechanism are fundamentally different from those responsible for the GGT in the RE-based MGs.

Acknowledgements

This research was supported by National Natural Science Foundation of China (Nos. 51671018, 51671021, 51531001, 11790293, 51871016 and 51871054), 111 Project (B07003), the Program for Changjiang Scholars and Innovative Research Team in University of China(IRT_14R05), International S&T Cooperation Program of China (2015DFG52600) and the Projects of SKL-AMM-USTB (2018Z-19). In situ high pressure XRD experiments were carried out at the beamline 16-ID-B and 16-ID-B APS, ANL, and also at the beamline 12.2.2, ALS, LBNL. EXAFS experiments were performed at beamline 20-BM-B, APS, ANL, and at beamline BL01C2, in NSRRC, Taiwan. Beamline 20-BM-B is supported by APS and the Canadian Light Source. APS is supported by DOE Office of Science (DE-AC02-06CH11357). ALS is supported by the Director, Office of Science, DOE-BES under Contract No. DE-AC02-05CH11231.

References

[1] Mishima, L. D. Calvert, and E. Whalley, Nature **314**, 76 (1985).

[2] R. J. Hemley, A. P. Jephcoat, H. K. Mao, L. C. Ming, and M. H. Manghnani, Nature **334**, 52 (1988).

[3] K. Miyauchi, J. Qiu, M. Shojiya, Y. Kawamoto, and N. Kitamura, Mater. Res. Bull., **34**, 1383 (1999).

[4] M. van Thiel and F. H. Ree, Phys. Rev. B **48**, 3591 (1993).

[5] T. Rouxel, H. Ji, T. Hammouda, and A. Moreac, Phys. Rev. Lett. **100**, 225501 (2008).

[6] H. W. Sheng, H. Z. Liu, Y. Q. Cheng, J. Wen, P. L. Lee, W. K. Luo, S. D. Shastri, and E. Ma, Nat Mater. **6**, 192 (2007).

[7] Q. S. Zeng, Y. C. Li, C. M Feng, P. Liermann, M. Somayazulu, G. Y. Shen, H. -k. Mao, R. Yang, J. Liu, T. D. Hu, and J. Z. Jiang, PNAS **104**, 13565 (2007).

[8] Q. S. Zeng, Y. Ding, W. L. Mao, W. Yang, S. V. Sinogeikin, J. Shu, H.-k. Mao, and J. Z. Jiang, Phys. Rev. Lett. **104**, 105702 (2010).

[9] M. J. Duarte, P. Bruna, E. Pineda, D. Crespo, G. Garbarino, R. Verbeni, K. Zhao, W. H. Wang, A. H. Romero, and J. Serrano, Phys. Rev. B **84**, 224116 (2011).

[10] G. Li, Y. Y. Wang, P. K. Liaw, Y. C. Li, and R. P. Liu, Phys. Rev. Lett. **109**, 125501 (2012).

[11] H. B. Lou, Y. K. Fang, Q. S. Zeng, Y. H. Lu, X. D. Wang, Q. P. Cao, K. Yang, X. H. Yu, L. Zheng, Y. D. Zhao, W. S. Chu, T. D. Hu, Z. Y. Wu, R. Ahuja and J. Z. Jiang, Sci. Rep. **2**, 376 (2012).

[12] Y. Y. Wang, W. Zhao, G. Li, Y. C. Li, and R. P. Liu, Mater. Lett. **110**, 184 (2013).

[13] F. Decremps, G. Morard, G. Garbarino, and M. Casula, Phys. Rev. B **93**, 054209 (2016).

[14] M. Wu, H. Lou, J. S. Tse, H. Liu, Y. Pan, K. Takahama, T. Matsuoka, K. Shimizu, and J. Z. Jiang, Phys. Rev. B **94**, 054201 (2016).

[15] L. Li, Luo, R. Li, H. Zhao, K. W. Chapman, P. J. Chupas, L. Wang, and H. Liu, Sci. Rep. **7**, 46762 (2017).

[16] Y. Y. Wang, X. Dong, X. Song, X. P. Li, and G. Li, Mater. Lett. **192**, 142 (2017).

[17] L. Zhang, F. Sun, X. G. Hong, J. L. Wang, G. Liu, L. P. Kong, H. W. Yang, X. R. liu, Y. Zhao and W. G. Yang, J. Alloy Compd. **695**, 1180 (2017).

[18] Q. Luo, G. Garbarino, B. A. Sun, D. W. Fan, Y. Zhang, Z. Wang, Y. J. Sun, J. Jiao,

X. D. Li, P. S. Li, N. Mattern, J. Eckert and J. Shen, Nat. Commun. **6**, 5703 (2015).

[19] Q. Zeng, Z. Zeng, H. Lou, Y. Kono, B. Zhang, C. Kenney-Benson, C. Park, and W. L. Mao., Appl. Phys. Lett. **110**, 221902 (2017).

[20] H. K. Mao, J. Xu, and P. M. Bell, J. Geophy. Res. **91**, 4673 (1986).

[21] D. Errandonea, A. Muñoz, and J. Gonzalez-Platas, J. Appl. Phys. **115,** 216101 (2014).

[22] B. N. Ravel, M., J. Synchrotron Radiat. **12**, 5 (2005).

[23] A. S. Nowick, Anelastic relaxation in crystalline solids. (Elsevier, 2012).

[24] G. Kresse and J. Furthmüller, Phys. Rev. B **54**, 11169 (1996).

[25] G. Kresse and D. Joubert, Phys. Rev. B **59**, 1758 (1999).

[26] K. Momma and F. Izumi, J. Appl. Crystallogr., **44**, 1272 (2011).

[27] D. Ma, A. D. Stoica, and X. L. Wang, Nat. Mater. **8**, 30 (2008).

[28] A. R. Yavari, A. L. Moulec, A. Inoue, N. Nishiyama, N. Lupu, E. Matsubara, W. J. Botta, G. Vaughan, M. D. Michiel and A. Kvick, Acta Mater. **53**, 1611 (2005).

[29] F. Birch, J. Geophys. Res. **57**, 227 (1952)

[30] J. D. Bass, Mineral Physics and Crystallography (American Geophysical Union, Washington DC, 1995).

[31] W. A. Bassett, T. Takahashi, H. K. Mao, and J. S. Weaver, J. Appl. Phys. **39**, 319 (1968).

[32] X. Chen and Y. Ma, EPL (Europhysics Letters) **100**, 26005 (2012).

[33] T. Takeuchi, D. Fukamaki, H. Miyazaki, K. Soda, M. Hasegawa, H. Sato, U. Mizutani, T. Ito, and S. Kimura., Materials Transactions **48**, 1292 (2007).

[34] P. F. Guan, T. Fujita, A. Hirata, Y. H. Liu, and M. W. Chen, Phys. Rev. Lett. **108**, 175501 (2012).

[35] V. Kumar, T. Fujita, K. Konno, M. Matsuura, M. W. Chen, A. Inoue, and Y. Kawazoe, Phys. Rev. B **84** 134204 (2011).

[36] A. D. Becke and K. E. Edgecombe, J. Chem. Phys. **92**, 5397 (1990).

[37] B.Zhang, R. J. Wang, and W. H. Wang, Phys. Rev. B **72**, 104205 (2005).

Captions

Figure 1 (Color online). ***In-situ* x-ray diffraction patterns of the $Pd_{41.5}Ni_{41.5}P_{17}$ MG under pressures at room temperature and the related volume dependence on pressure. (a)** The *in-situ* high-pressure XRD experiments were conducted in methanol-ethanol mixture and helium, respectively. The position of the first sharp diffraction peak (FSDP) shifts to higher angles with the increase of pressure, as pointed out by the arrows. **(b)** The change of relative volume as a function of the pressure. Data points are derived from the FSDP position. Two distinct states, below 6 GPa (dashed black line) and above 6 GPa (dashed red line) with an inflection point are identified. The repeatability of this unique GGT phenomenon was confirmed by two sets of data using different pressure mediums, i.e., helium and the methanol-ethanol mixture.

Figure 2 (Color online). **Reliability of the calculated structure of the $Pd_{41.5}Ni_{41.5}P_{17}$ glass at ambient temperature and pressure. (a)** The simulated atomic configuration. The green, blue and pink balls represent Pd, Ni and P, respectively. **(b)** The calculated PDF (red line) and the experimental one (open circle). **(c)** The EXAFS spectra from the simulated atomic configurations (solid line) and experimental data (open symbols). **(d)** The Fourier transformation profile of the experimental EXAFS spectra and calculated ones.

Figure 3 (Color online). **The total and the projected densities of states (DOS) for the $Pd_{41.5}Ni_{41.5}P_{17}$ metallic glass at zero and 78 GPa. (a)** Total DOS. **(b-d)** PDOS plots for Pd, P and Ni, respectively.

Figure 4 (Color online). **Quantitative analysis of the different charge density distribution in the $Pd_{41.5}Ni_{41.5}P_{17}$ metallic glass under different pressure. (a)** 0 GPa. **(b)** 23 GPa. **(c)** 41 GPa. **(d)** 78 GPa.

Figure 5 (Color online). **Quantitative analysis of the ELF in the $Pd_{41.5}Ni_{41.5}P_{17}$ metallic glass under different pressures. (a)** 0 GPa. **(b)** 23 GPa. **(c)** 41 GPa. **(d)** 78 GPa.

Figure 6 (Color online). **Simulated pressure-dependent total and partial PDFs of $Pd_{41.5}Ni_{41.5}P_{17}$ metallic glass under pressure up to 78 GPa. (a)** Total PDFs. **(b)** Partial PDFs of P-(Pd, Ni) atomic pairs. **(c)** Partial PDFs of Ni-(Pd, Ni) atomic pair. (**d)** Partial PDFs of Pd-(Pd, Ni) atomic pair.

Figure 7 (Color online)**. XRD patterns of the $Pd_{41.5}Ni_{41.5}P_{15}$ MGs at different pressure states, i.e., before pressurization, 10.5(1) GPa and after pressure release.**

Table I. Parameters of the Birch-Murnaghan Equation of State for the $Pd_{41.5}Ni_{41.5}P_{17}$ MG before and after the GGT.

Fig. 1 by Du et al.

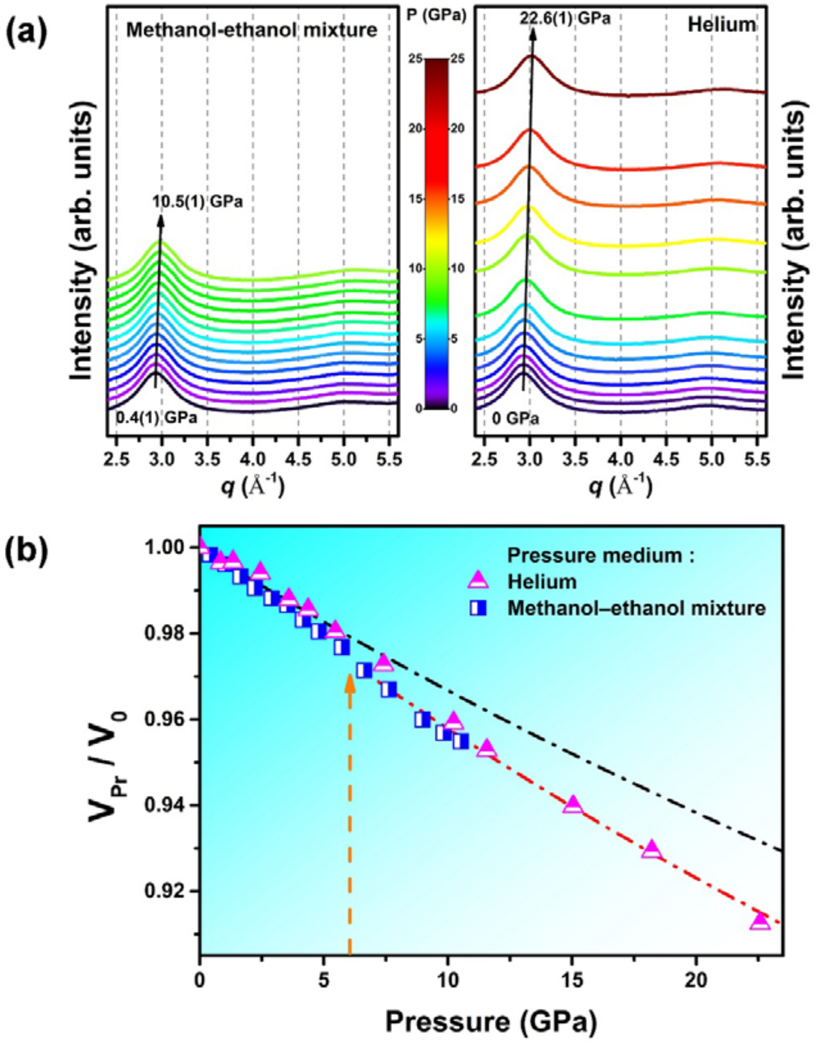

Fig. 2 by Du *et al.*

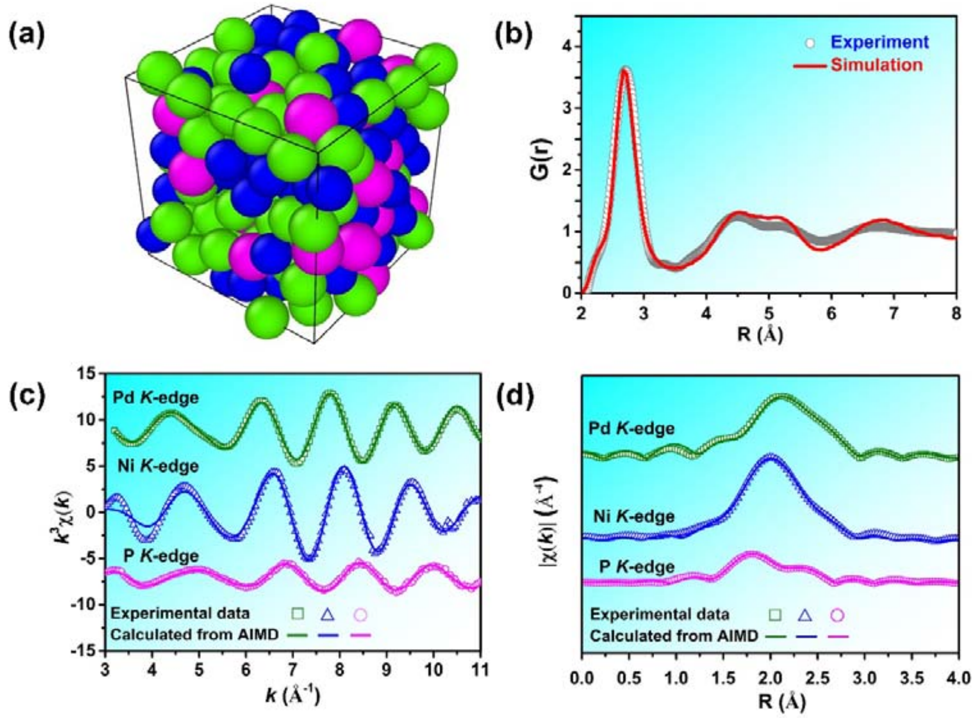

Fig. 3 by Du *et al.*

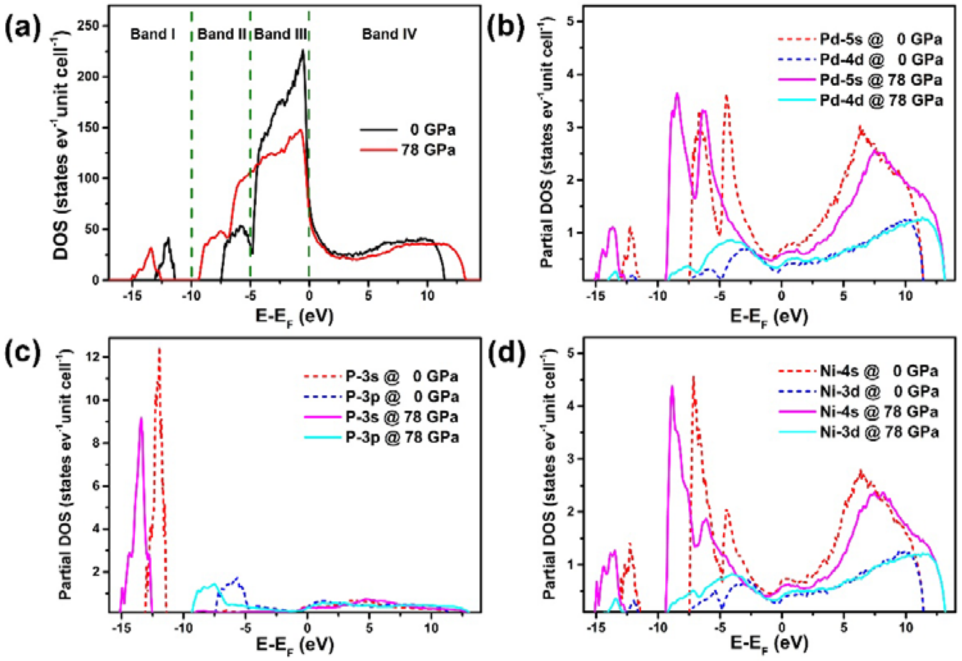

Fig. 4 by Du et al.

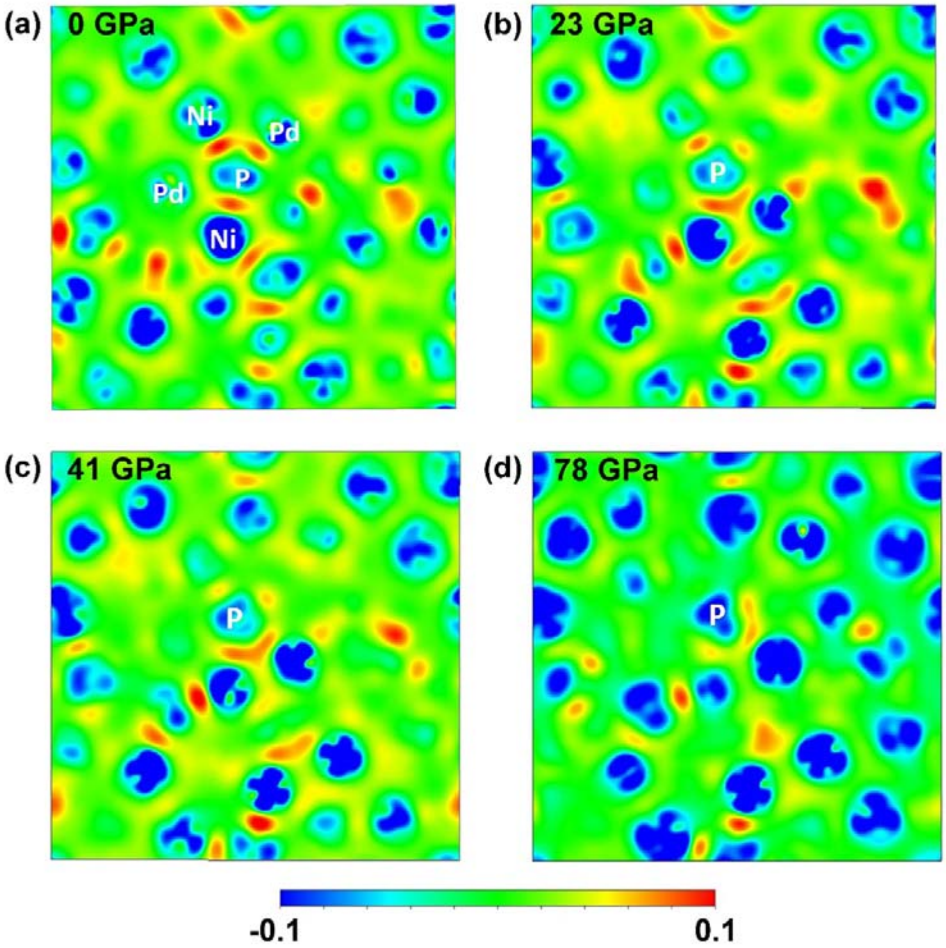

Fig. 5 by Du *et al.*

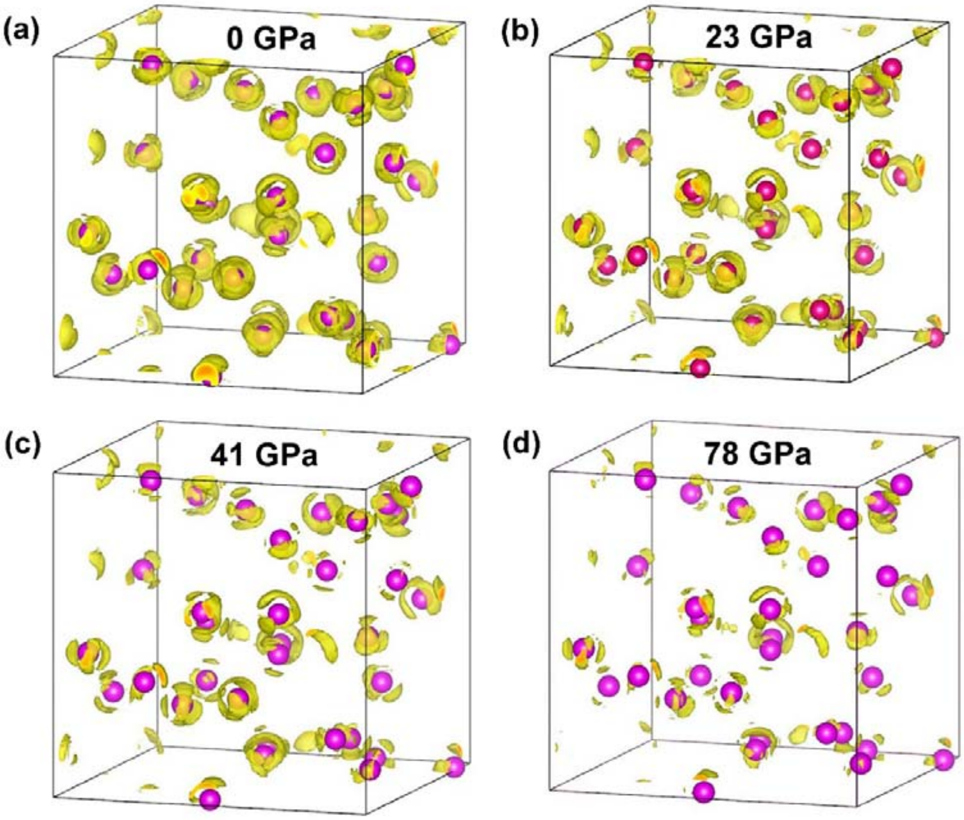

Fig. 6 by Du et al.

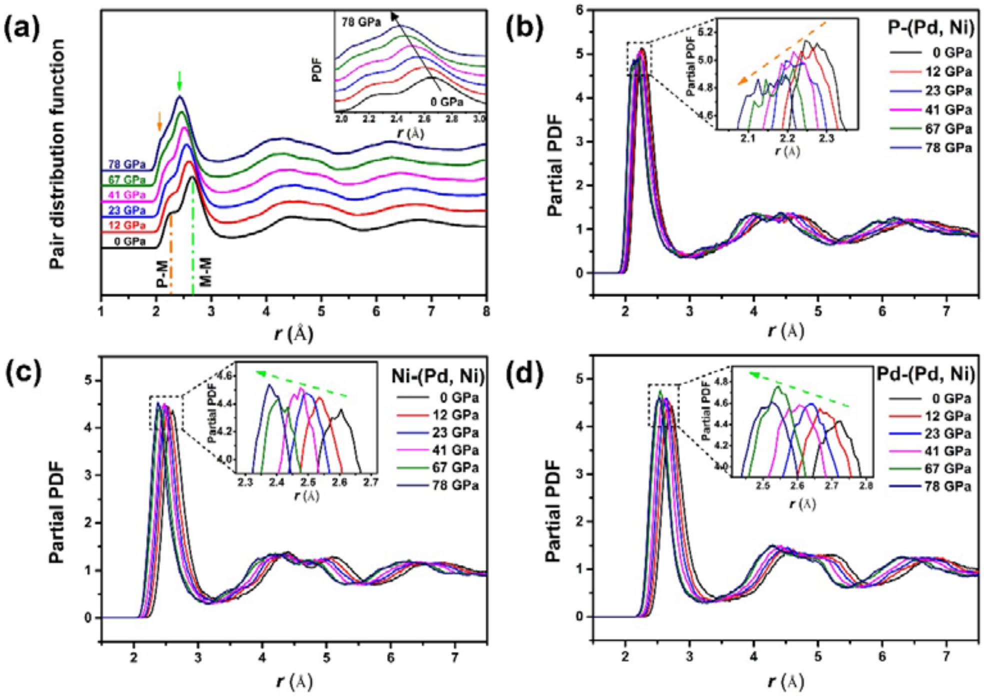

Fig. 7 by Du et al.

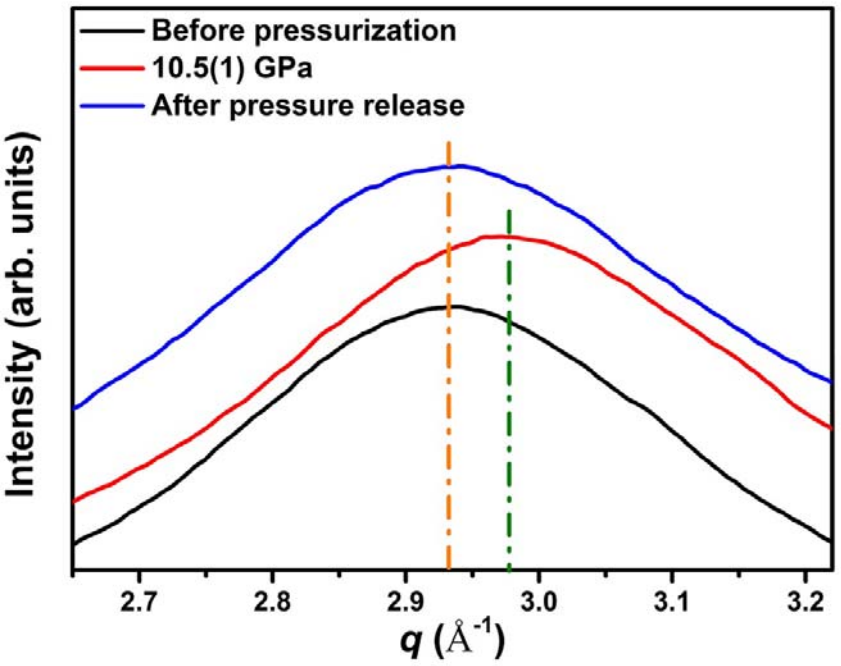

Table. I by Du *et al.*

Glass state	B_0	Reduced chi-square	R-square	B_0'
EOS below 6 GPa	288(5)	0.01	0.997	4 (fixed)
EOS above 6 GPa	210(2)	0.21	0.991	4 (fixed)